Analytic Theory of the Resonance Properties of Metallic Nanoslit Arrays

Jae Woong Yoon, Myoung Jin Jung, Seok Ho Song, and Robert Magnusson, *Senior Member, IEEE*

***Abstract*— By applying formulation based on time reversibility, we provide the analytic theory of resonance properties of metallic nanoslit arrays. We model lossy resonant systems in which a resonance is induced by a single quasi-bound mode (QBM). It is consistent with the Fano resonance theory of quantum interference of auto-ionizing atoms and captures the essential characteristics of dissipative resonant systems. We show that time-reversibility requirements lead to analytical solutions for the resonant transmission and the associated nonreciprocal absorption in terms of a minimal number of independent basic parameters that include partial decay probabilities of resonant pathways and the non-resonant transmission amplitude. With a clear view of interfering electromagnetic field configurations and the associated absorbing processes, the theory reveals the essential physics of resonant optical transmission. In particular, the enhanced transmission peak is given by the product of partial decay probabilities and is independent of the non-resonant light wave amplitude. In a highly asymmetric coupling regime, the excitation of the QBM leads to anti-resonant extinction of the transmission, indicating a negative role of the QBM. The parity of the QBM determines occurrence of red or blue tails in the spectral profile. Absorbance measurements yield direct determination of the partial decay probabilities by which the main features of the resonant transmission are quantitatively explained. Thus, these basic parameters can be directly established experimentally. Full numerical calculations of the transmission spectra are in complete quantitative agreement with our analytical formulation for optical transmission mediated by both slit cavity modes and plasmonic modes.**

***Index Terms*— Analytical models, nanostructured materials, periodic structures, resonance light scattering.**

I. Introduction

NANOPATTERNED surfaces with subwavelength periodicity are of immense interest for various potential applications. In particular, periodic metallic films support resonant energy localization and associated extraordinary optical transmission (EOT) [1], [2]. The resonance mechanisms behind EOT have been widely discussed in the literature and generally have been found to correspond to surface-plasmon polaritons (SPP) and Fabry-Pérot cavity modes [3]. We recently provided normalized parametric maps for an example idealized metal film with narrow slits, rendering clearly the regimes of dominance for these mechanisms [4].

In this paper, we treat the resonance interactions in detail, formulating their properties in terms of basic physical parameters. We model a nanostructured metal film as a dissipative quasi-bound resonator where the resonant (indirect) and non-resonant (direct) scattering pathways interfere. We apply the phenomenological coupled-mode theory due to Haus [5] to obtain the attendant transmission, reflection, and absorption spectra. For a resonance interaction that can derive from SPP or cavity mode, we find an analytic expression for the transmission spectrum in terms of the non-resonant transmission field amplitude and the radiation yields of the localized mode expressed in terms of relevant decay probabilities. We present numerical results obtained by rigorous coupled-wave analysis (RCWA) that show excellent agreement with the analytic theory.

The interference picture of EOT, i.e., Fano-type interpretation, has been accepted as a general explanation of the characteristic asymmetric spectral profile and red-shifted transmission peak [6], [7]. In the absence of an available theory that analytically decomposes the two interfering electromagnetic (EM) field configurations, numerical fitting typically applies this picture to experimental or simulated spectra [6], [8]. As the detailed information is implicitly held in the fitted phenomenological parameters, the interference picture associated with the formal quantum Hamiltonian mapping does not describe any further physics involved in the EM field interaction. Hence, to ameliorate this, we provide an analytic theory that clearly defines the two interfering EM field configurations in terms of basic parameters such as the non-resonant scattering amplitudes and partial radiation yields. We show that the basic parameters can be experimentally determined by absorbance measurements. The essential features of EOT, such as the enhanced maximum and anti-resonant extinction, are quantitatively described by a simple analytic formula.

II. Fano Profile and Time Reversibility

As discussed by Genet *et al.* [6], EOT can be explained as a resonant light scattering process where Fano interference takes place between two transmission pathways: the resonant pathway mediated by a discrete state, e.g., SPP [1], [9] or cavity mode [2], and the non-resonant pathway via a

Manuscript received January 11, 2012; revised March 20, 2012; accepted March 24, 2012. Date of publication April 3, 2012; date of current version May 8, 2012. This work was supported in part by the National Research Foundation of Korea Grant funded by the Korea Government MEST under Grant 2010-000256, the ERC Program of Optics and Photonics Elite Research Academy, and the Texas Instruments Distinguished University Chair in Nanoelectronics endowment.

J. W. Yoon and R. Magnusson are with the Deparment of Electrical Engineering, University of Texas-Arlington, Arlington, TX 76019 USA (e-mail: jaeyoon@uta.edu; magnusson@uta.edu).

M. J. Jung and S. H. Song (corresponding author) are with the Department of Physics, Hanyang University, Seoul 133-791, Korea (e-mail: makeit0@hanyang.ac.kr; shsong@ hanyang.ac.kr).

Color versions of one or more of the figures in this paper are available online at http://ieeexplore.ieee.org.

Digital Object Identifier 10.1109/JQE.2012.2192914

continuum, analogous to Bethe's contribution for hole arrays [10]. According to the Fano resonance interpretation of EOT, the transmitted intensity is given by an expression similar to that originally found for the quantum interference of an auto-ionizing atom as [6], [11]

$$T(\delta) = |t_D|^2 \frac{(q+\delta)^2}{1+\delta^2}, \tag{1}$$

where the reduced frequency is $\delta = (\omega - \omega_0)/\gamma_{tot}$ for a discrete state at $\omega_0 + i\gamma_{tot}$ and t_D is a transition probability amplitude via the continuum. The shape factor q describes resonant interference features such that the resonant enhancement is $T_{max} = |t_D|^2(q^2+1)$ at $\delta = 1/q$ and the anti-resonant extinction is $T_{min} = 0$ at $\delta = -q$. The universal applicability of Eq. (1) to classical resonance phenomena is of interest in nanophotonics and plasmonics [12]. However, the formal quantum Hamiltonian mapping does not clearly reveal the EM field configurations associated with the two interfering pathways [6], [13] and does not contain realistic absorbing processes as the probability flux is always conserved. Therefore, the Fano interference picture of EOT is incomplete. In particular, it is unclear how to define q exactly, how to associate the non-reciprocal absorbance A and reflectance R with the reciprocal transmittance T, and how to optimize T_{max} and T_{min} in a real material system. The objective of this paper is to bridge this gap.

Time reversibility is a fundamental property that we use to link Eq. (1) for quantum interference to classical resonance problems. In the frequency domain, time reversibility of EM field scattering is dictated by the conjugation invariance (C-invariance) of Maxwell's equations [14]. With incoming and outgoing asymptotic modes represented by $|\psi_+\rangle$ and $|\psi_-\rangle$, respectively, the C-invariance implies that the scattering matrix equation $|\psi_-\rangle = S(\varepsilon)|\psi_+\rangle$ is consistent with its time-reversed form $|\psi_+\rangle^* = S(\varepsilon^*)|\psi_-\rangle^*$, i.e. [14], [15],

$$S^{-1}(\varepsilon) = S^*(\varepsilon^*). \tag{2}$$

We refer to this property as *quasi reversibility* because the loss-gain replacement ($\varepsilon \rightarrow \varepsilon^*$) involved in the time reversal operation is forbidden by the second law of thermodynamics at macroscopic levels. As reported recently, coherent absorption of light is described by the exact time reversal of the lasing process using this quasi-reversibility argument [15]. In this paper, we prove that Eq. (2) correlates the phase difference and amplitude ratio of the EM fields pertaining to the two interfering pathways. The interference picture of EOT on this basis analytically decomposes the field configurations associated with the two interfering pathways in dissipative material systems, thereby yielding clear, improved Fano-type interpretation of this resonance effect.

III. Analytic Theory of EOT Based on Quasi-Reversibility Arguments

We use a coupled-mode model schematically shown in Fig. 1(a). A resonant transfer of light involving a discrete state (blue arrows with coupling rates κ_1 and κ_2) occurs on the coupling of an incident wave to a quasi-bound mode (QBM) resonant at $\omega_0 + i\gamma_{tot}$ and its re-emission to both sides of the

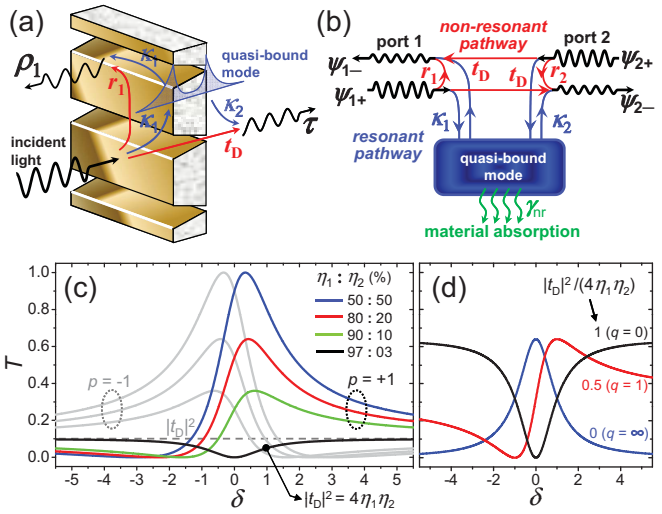

Fig. 1. (a) Schematic of scattering processes modeled as resonant (blue arrows with coupling rates κ_1 and κ_2) and non-resonant (red arrows with coupling amplitudes r_1 and t_D) pathways. (b) Two-port resonator system modeling the scattering processes in (a) (r_2 is non-resonant reflection amplitude at port 2). The non-radiative decay rate γ_{nr} (green arrows) describes material losses in the resonant pathway. (c) Dependence of transmittance T on the QBM's partial decay probabilities (η_1 and η_2). Gray curves represent T spectra for odd parity ($p = -1$). Note that $T_{max} = 1$ for $\eta_1 = \eta_2$ (blue) and asymmetry in η_n results in reduced transmission maxima. (d) Dependence of the T spectrum on the ratio of the non-resonant contribution to the resonant contribution, i.e., $|t_D|^2/(4\eta_1\eta_2)$. The curves are marked by the corresponding shape factor q.

film. Here, t_D and r_1 represent direct (non-resonant) transmission and reflection amplitudes of the continuum input (red arrows), respectively. This coupled-mode interaction is framed as a two-port resonator system shown in Fig. 1(b) where the QBM couples to two radiation ports and dissipates its energy to material losses via a non-radiative decay process (green arrows with decay rate γ_{nr}). As shown in APPENDIX A, in a slowly decaying regime where $\gamma_{tot} << \omega_0$, applying coupled-mode theory [5], [14], [16], the transmission coefficient is

$$\tau(\delta) = t_D + \frac{2\sqrt{\eta_1\eta_2}}{1 - i\delta} e^{i\phi} \equiv t_D + t_R(\delta), \tag{3}$$

where $\phi = \arg(\kappa_1) + \arg(\kappa_2)$ is the resonant transfer phase at $\delta = 0$, $\eta_n = |\kappa_n|^2/(2\gamma_{tot})$ is the partial decay probability of the QBM to port n, and $\gamma_{tot} = |\kappa_1|^2/2 + |\kappa_2|^2/2 + \gamma_{nr}$ is the total decay rate. The decay probabilities η_n associated with the decay rates γ satisfy $\eta_1 + \eta_2 + \eta_{nr} = 1$ with $\gamma_{nr} = \eta_{nr}\gamma_{tot}$ and $\gamma_n = \eta_n\gamma_{tot}$. Fano-type interference between the non-resonant t_D and the resonant $t_R(\delta)$ transfer amplitudes is explicit in Eq. (3). The transmitted intensity $T = |\tau|^2 = |t_D|^2 + |t_R|^2 + 2\mathrm{Re}(t_D \cdot t_R^*)$ becomes fully deterministic with minimal parameters of $|t_D|$ and η_n once the phase difference between t_D and t_R is known.

As shown in APPENDIX B, there are two main consequences of Eq. (2). First, the amplitude ratio $|t_D/t_R(0)|$ and phase difference $\Delta = \arg[t_D] - \arg[t_R(0)]$ are related by

$$\cos\Delta = -\eta_{rad}\left|t_D / t_R(0)\right|, \quad \sin\Delta = p\sqrt{1 - \cos^2\Delta}, \tag{4}$$

where $\eta_{rad} = \eta_1 + \eta_2$ is the total radiation yield and p is the parity of the QMB assigned $p = +1$ to an even-like mode

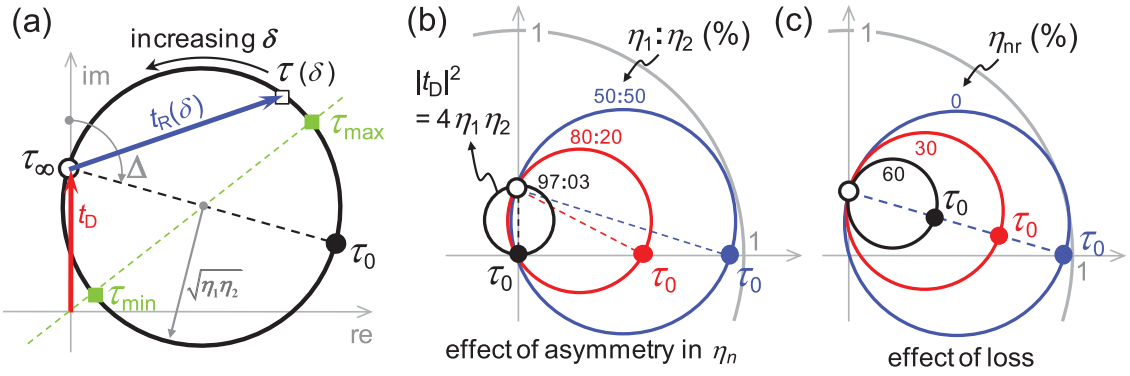

Fig. 2. (a) Geometry of a resonance response circle (RRC). $\tau(\delta)$ is the superposition of the resonant (blue arrow) and non-resonant (red arrow) contributions tracing the black circle starting from τ_∞ at $\delta = -\infty$ (far off resonance), passing through τ_0 at $\delta = 0$ (on resonance), and going again to τ_∞ at $\delta = +\infty$ (far off resonance). $\tau_{\max}$ and $\tau_{\min}$ denote the enhanced transmission maximum at $\delta = 1/q$ and the anti-resonant extinction at $\delta = -q$, respectively. Non-resonant transmission phase, $\arg(t_D)$, is fixed at $\pi/2$ for simplicity. (b) Dependence of RRC on partial decay probabilities η_1 and η_2 for ports 1 and 2. Blue, red, and black RRCs correspond to the spectrum in Fig. 1(c) with the same color scheme and show amplitude-phase correlation as diameter-inclination correlation. The black circle shows that the condition $|t_D| = |t_R(0)|$ leads to π phase jump and associated $T = 0$ at resonance $\delta = 0$. (c) Dependence of RRC on QBM's loss. As the absorbing probability η_{nr} increases, the RRC diameter shrinks with its inclination Δ being constant.

and $p = -1$ to an odd-like mode. Second, the nonreciprocal absorbance for light entering port n is expressible as

$$A_n(\delta) = \frac{4\eta_n\eta_{nr}}{1+\delta^2}, \tag{5}$$

when $\eta_1 \neq \eta_2$, where the probability of absorption is $\eta_{nr} = 1-\eta_{rad} = 1-\eta_1-\eta_2$.

Eqs. (3)–(5) reveal the essential physics of Fano interference in EOT and connect well with the paper by Genet *et al.* [6]. For lossless resonance systems, Eq. (3) reduces to Eq. (1) with the shape factor q now expressed as

$$q = p\sqrt{4\eta_1\eta_2 \Big/ |t_D|^2 - 1}. \tag{6}$$

The following properties emerge clearly: (i) the QBM's parity p determines whether a blue tail ($q > 0$) or a red tail ($q < 0$) is observed in the spectrum [6], [11]; (ii) the enhanced transmission maximum is $T_{\max} = |t_D|^2(q^2+1) = 4\eta_1\eta_2$, independent of the non-resonant expectation $|t_D|^2$, e.g., standard aperture theory by Bethe [10]; (iii) a symmetric enhancement peak arises for $q = \pm\infty$, which is obtained when $t_D = 0$, showing that nonzero t_D causes the spectral asymmetry; (iv) a balance between the resonant and non-resonant contributions such that $4\eta_1\eta_2 \approx |t_D|^2$ results in a symmetric extinction dip with $q = 0$, i.e., the QBM plays a negative role [17]. Figs. 1(c) and 1(d) illustrate the arguments (i)–(iv); these are computed by using Eqs. (3) and (4).

Representing Eq. (3) in the complex plane provides an intuitive understanding of the resonant interference. In Fig. 2(a), $\tau(\delta)$ given by Eq. (3) is a circle with radius $(\eta_1\eta_2)^{1/2}$, its far off-resonance end $\tau(\infty)$ $(= \tau_\infty)$ lifted by t_D, and its axis connecting τ_∞ and $\tau(0)$ $(= \tau_0)$ inclined counter-clockwise by Δ from the axis parallel to t_D. We refer to this circle as a resonance response circle (RRC). With the RRC representation of $\tau(\delta)$ in Fig. 2(a), the transmission maximum at $\delta = 1/q$ and minimum at $\delta = -q$ are geometrically determined by $\tau_{\max}$ and $\tau_{\min}$ at which the green line connecting the center of the RRC and the origin crosses the RRC.

In lossless cases, the amplitude-phase correlation in Eq. (4) is clearly visualized in the RRC as a geometric connection between its diameter and inclination. The phase difference between the non-resonant and resonant contributions Δ is determined so that the RRC always passes through the origin. Fig. 2(b) with corresponding spectra in Fig. 1(c) shows how amplitude-phase correlation affects the RRC and the T spectrum. For a lossless system, anti-resonant null transmission is inevitable, i.e., $T_{\min} = |\tau_{\min}|^2 = 0$, and $T_{\max}$ must be a square of RRC's diameter, i.e., $T_{\max} = |\tau_{\max}|^2 = 4\eta_1\eta_2$. We note that $\eta_1 = \eta_2 = 0.5$ is necessary for $T_{\max} = 1$. It means that a lossless symmetric structure, e.g., a free-standing film in a resonant coupling regime, must exhibit a full transmission peak [2], [18], [19]; complete transmission is also obtainable even in an asymmetric system such as glass-supported films with conical holes or trapezoidal slits that balance the radiation yields of an SPP to each side of the film.

Increasing loss (γ_{nr}) without affecting κ_n results in reduced RRC radius, $(\eta_1\eta_2)^{1/2} = |\kappa_1\kappa_2|/(|\kappa_1|^2 + |\kappa_2|^2 + 2\gamma_{nr})^{1/2}$, while Δ remains constant as shown in Fig. 2(c). Thus, the material loss suppresses $T_{\max}$ while $T_{\min}$ increases from zero because the RRC does not pass through the origin anymore. Note that Eq. (1) is not strictly valid with material losses. In particular, loss appreciably degrades $T_{\max}$, but the destructive interference effect at $T_{\min}$ is persistent for the low $|t_D|$ regime with $T_{\min} \approx \eta_{nr}^2|t_D|^4/T_{\max}$, which is far below the spectral background level $|t_D|^2$.

In dissipative films, even small loss coefficients may yield strong absorption when the system becomes resonant due to excitation of a QBM. Thus, absorption plays an important role in EOT [14], [20]. A main consequence of resonant absorption is nonreciprocity in the absorbance and reflectance for an asymmetric system [20], e.g., glass-supported films. From Eq. (5), the on-resonance (peak) absorbance is $A_n(0) = 4\eta_n\eta_{nr}$. Thus, quantitative nonreciprocity is expressible as $|A_1(0)-A_2(0)| = 4\eta_{nr}|\eta_1-\eta_2|$. Nonreciprocity in R_n must be identical to that in A_n because reflectance $R_n = 1-T-A_n$ and T is reciprocal in principle. The nonreciprocity measures the

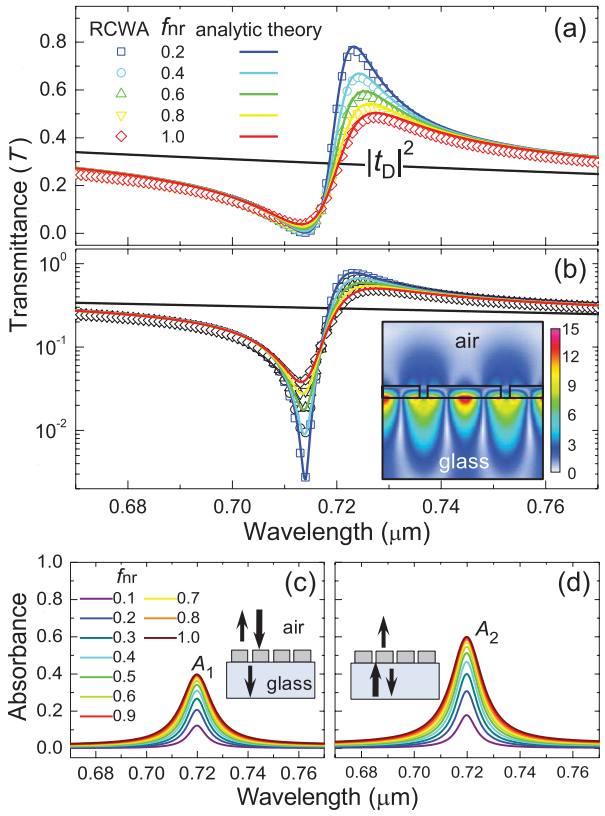

Fig. 3. Numerically computed resonant transmission and absorption due to an SPP excitation in a 1-D array of metallic nanoslits on glass substrate ($n = 1.5$). The metal film thickness $d = 40$ nm, array period $\Lambda = 400$ nm, and slit width w = 20 nm. (a) Transmission spectra for absorption factors $f_{nr} = 0.2$ (blue), 0.4 (cyan), 0.6 (green), 0.8 (yellow), and 1.0 (red). (b) Re-plot of (a) on a log scale. Absorption spectra for (c) air-side light incidence (A_1) and (d) glass-side light incidence (A_2), where line colors represent different absorption factors $f_{nr} = 0.1$-1. In (a) and (b), symbols represent RCWA calculation results and solid curves are found by the analytic theory. Inset in (b) shows magnetic field distribution, $|H/H_0|$, at $\lambda = 0.72$ μm.

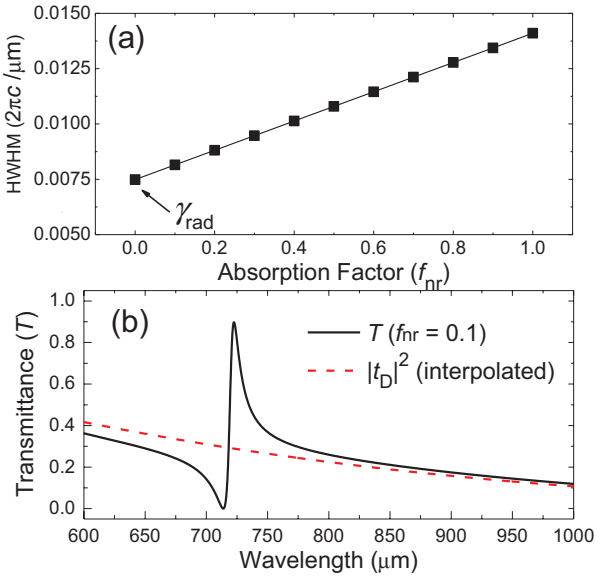

Fig. 4. (a) Linear dependence of total decay rate γ_{tot} (HWHM) of the SPP in Fig. 3 on absorption factor f_{nr}. (b) Transmission spectrum (RCWA) for $f_{nr} = 0.1$ (black solid curve) and the interpolated non-resonant transmittance $|t_D|^2$ (red dashed curve).

difference in the QBM decay probability coefficients (radiation yields) η_n and, therefore, directly relates to T_{max}, which takes small values under highly asymmetric η_n as seen in Fig. 1(c). Based on Eq. (5), the lossless limit of T_{max} can be expressed in terms of A_n as

$$\lim_{\eta_{nr}\to 0} T_{max} = M = 4\gamma_1\gamma_2/\gamma_{rad}^2 = 4A_1A_2/(A_1+A_2)^2. \quad (7)$$

Thus T_{max} for the lossless case is extracted from the lossy array. Equation (7) states that even for a lossless metal, T_{max} is generally not unity.

IV. Surface-Plasmonic EOT

We quantitatively check our theory with full numerical calculations [21]. The film is modeled as a Drude metal with collision and plasma frequency, $\Gamma = 4.52 f_{nr}\times 10^{13}$ rad/s and $\omega_p = 7.54\times 10^{15}$ rad/s, respectively, where f_{nr} is an absorption factor. Frequency-dependent dielectric constant of the metal is given by $\varepsilon_{metal}(\omega) = 1 - \omega_p^2(\omega^2 + i\Gamma\omega)^{-1}$. The absorption factor f_{nr} adjusts the collision frequency of free electrons in the Drude metal such that γ_{nr} of a mode supported by a metallic system is directly proportional to it [23]. Surface normal incidence is assumed.

For an optically thin film with slit cavity length short enough to thwart cavity mode (CM) resonance, an SPP at either interface of the film can operate as a dominant transmission-enhancing QBM [4]. For a thin metal film with thickness comparable to the skin depth, the metal film allows non-resonant transmission directly through it. Thus, Fano-type interference between the resonant and non-resonant pathways leads to a transmission spectrum highly asymmetric exhibiting an enhanced transmission peak and an anti-resonant extinction dip.

Fig. 3 shows numerical results for an optically thin nanoslit array with thickness d = 40 nm, period $\Lambda = 400$ nm, and slit width w = 20 nm. The resonance feature at 0.72 μm is attributed to the excitation of an SPP on the glass/metal interface. It is confirmed in the inset of Fig. 3(b) showing typical SPP character in the field near the glass/metal interface. The transmission spectra in Fig. 3(a) and a logarithmic re-plot in Fig. 3(b) clearly exhibit asymmetric profiles with T_{max} decreasing with increasing f_{nr}. In contrast to T_{max}, the anti-resonant dips (T_{min}) increase with f_{nr}. The effect of material absorption on T_{max} and T_{min} qualitatively agrees with the analytic theory description. Numerical absorption spectra are shown in Figs. 3(c) and (d).

To quantitatively verify the analytic theory, we extract from the computed absorbance spectra in Fig. 3 the basic resonance parameters (t_D, η_n, and η_{rad}) and compare the analytical and numerical spectral profiles. We first extract η_{rad} by measuring the half-width at half-maximum (HWHM) of the absorbance peaks. HWHM (γ_{tot}) measured from the simulated absorbance spectra (A_n) in Figs. 3(c) and 3(d) is indicated in Fig. 4(a). It confirms that γ_{tot} increases linearly with f_{nr}, implying $\gamma_{nr} \propto f_{nr}$. HWHM linearly extrapolated to $f_{nr} = 0$ is identified as γ_{rad} and, then, we find $\eta_{rad} = \gamma_{rad}/\gamma_{tot}$. This method is valid for

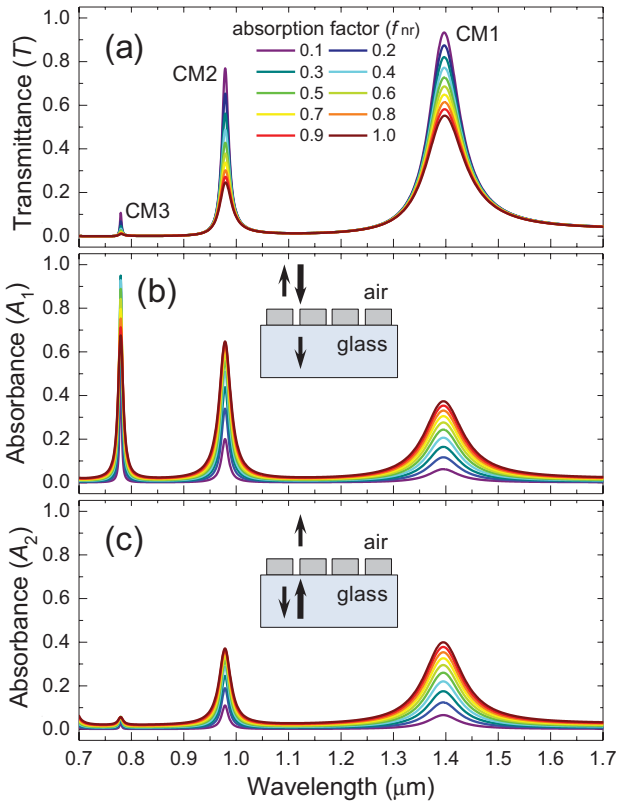

Fig. 5. Fig. 5. Numerical transmission and absorption spectra due to cavity mode excitation in a 1-D array of metallic nanoslits on glass substrate ($n = 1.5$). The metal film thickness d = 550 nm, array period $\Lambda = 400$ nm, and slit width w = 20 nm. (a) Transmission spectrum. Absorption spectra for (b) air-side light incidence (A_1) and (c) for glass-side light incidence (A_2). Line colors represent different absorption factors $f_{nr} = 0.1 - 1$ as indicated in (a).

most noble metals satisfying $|\mathrm{Re}(\varepsilon_{metal})| >> |\mathrm{Im}(\varepsilon_{metal})|$ [23]. We estimate partial radiation yield η_n by using

$$\eta_n = \eta_{rad} A_n/(A_1 + A_2). \tag{8}$$

This relation is found straightforwardly from Eq. (5). Except for $|t_D|$, all basic parameters for the analytic theory are obtained from the absorption spectra. We obtain the non-resonant transmittance $|t_D|^2$ by interpolating (4th-order polynomial) it from the RCWA calculated transmission spectrum for far-off resonant wavelength ranges. The interpolated $|t_D|^2$ is indicated by the red dashed curve in Fig. 4(b) and shown as black curves in Figs. 3(a) and 3(b).

The analytic theory curves in Figs. 3(a) and 3(b) are obtained by using partial radiation yields (η_{rad} and η_n) purely estimated from the absorbance spectra and $|t_D|^2$ interpolated from the off-resonant transmittance. Thus we confirm excellent quantitative agreement between the analytic theory and RCWA calculations in describing T_{max}, T_{min}, spectral profile, and their dependence on the material absorption.

V. Cavity-Modal EOT

For an optically thick metal film, resonant CMs inside the nanoslits [2]-[4], [13], [17] correspond to the QBM in our model. Fig. 5 shows transmission and absorption spectra calculated by RCWA for a nanoslit array with thickness

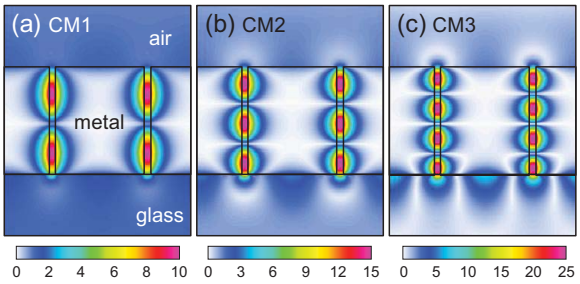

Fig. 6. Magnetic field distributions, $|H/H_0|$, at wavelengths (a) $\lambda = 1.395$ μm, (b) 0.978 μm, and (c) 0.779 μm for $f_{nr} = 0.1$.

d = 550 nm, period $\Lambda = 400$ nm, and slit width w = 20 nm. Three resonance features at wavelengths 0.779, 0.978, and 1.395 μm are due to Fabry-Pérot (FP) resonances of the cavity modes inside the nanoslits as confirmed by the associated field distributions in Fig. 6. We label each mode as CMl with l indicating the number of nodes inside the cavity.

Qualitative agreement with the analytic theory is observed from the transmission and nonreciprocal absorption [20], [22] spectra in Fig. 5. For CM1 with $A_1 \approx A_2$, implying $\eta_1 \approx \eta_2$ according to our analytic theory interpretation, the peak transmittance T_{max} is largest (0.934 for $f_{nr} = 0.1$) while T_{max} for CM3 with $A_1 >> A_2$, implying $\eta_1 >> \eta_2$, is much smaller (0.107 for $f_{nr} = 0.1$). One might prefer high absorption of CM3 in Fig. 5(b) as the main reason for its low T_{max}. This interpretation, however, cannot explain the small transmission peak of CM3 in case of light incidence from glass substrate in Fig. 5(c) where CM3 exhibits much smaller absorption than CM1.

The large difference between η_1 and η_2 for CM3 is due to its spectral proximity to the SPP resonance wavelength at the glass/metal interface. Note excitation of surface field at the glass/metal interface in Fig. 6(c). In our case, the glass/metal interface becomes resonant due to the excitation of SPP at 0.721 μm given by $\Lambda[\varepsilon_{glass}\varepsilon_{metal}/(\varepsilon_{glass}+\varepsilon_{metal})]^{1/2}$, where ε represents dielectric constant of the material indicated by its subscript. It is known in the literature [3] that the internal reflectance of a CM tends to 100% near the SPP resonance wavelength, suppressing coupling of the CM to the outside radiation. Thus, out-coupling of CM3 to glass substrate must be much smaller than that to air side, i.e., $\eta_1 >> \eta_2$.

We again apply the same analysis method as in Sec. IV to quantitatively check the validity of the analytic theory to a cavity modal EOT. Decay rates γ_{rad} for CM1~CM3 are obtained by linearly extrapolating HWHM of the absorbance peaks in Figs. 5(b) and 5(c). The result is presented in Fig. 7(a).

For an optically thick metal film, t_D is reasonably close to zero because there is no available transmission pathway other than the slit cavity. In this case, the analytic theory yields

$$T_{max} = 4\eta_1\eta_2 = M\eta_{rad}^2, \tag{9}$$

where M can be given in terms of peak absorbances according to Eq. (7). We obtain $M = 0.9995$ for CM1, 0.912 for CM2, and 0.184 for CM3 from the peak absorbance in

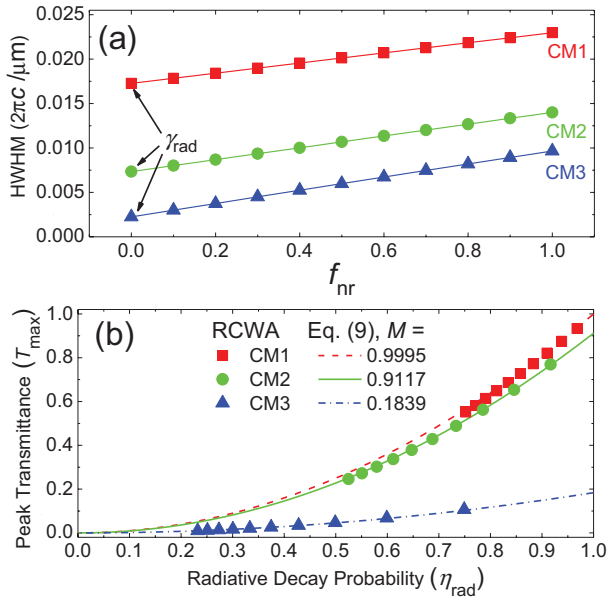

Fig. 7. (a) Total decay rate γ_{tot} (HWHM) versus absorption factor f_{nr} for CM1 (red squares), CM2 (green circles), and CM3 (blue triangles). γ_{rad} of each mode is inferred by linearly extrapolating γ_{tot} to $f_{nr} = 0$. (b) Peak transmittance T_{max} versus radiative decay probability η_{rad}, where symbols represent RCWA calculation results while solid curves represent Eq. (9) due to the analytic theory. Note that M is the value of T_{max} extrapolated to $\eta_{rad} = 1$ (corresponding to $\eta_{nr} = 0$).

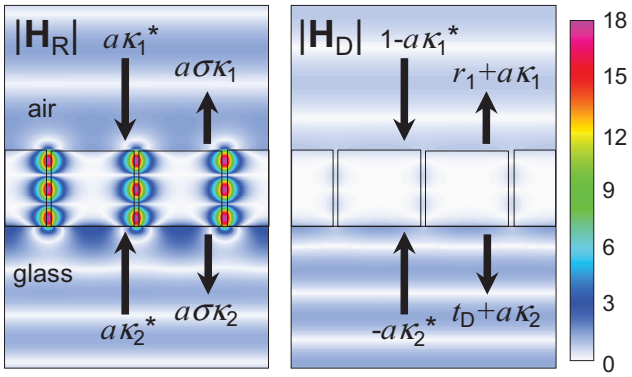

Fig. 8. Decomposition of the total field into resonant ($\mathbf{H}_R$) and non-resonant ($\mathbf{H}_D$) configurations for CM2 in Fig. 5. The total field $\mathbf{H}_{tot}$ is a superposition of the following: (left panel) $\mathbf{H}_R$ that completely describes the field associated with the QBM in $\mathbf{H}_{tot}$, (right panel) $\mathbf{H}_D$ that does not excite the QBM (cavity mode in this case). Note arrows and their amplitudes for coherent combinations of incoming and outgoing waves associated with $\mathbf{H}_D$ and $\mathbf{H}_R$.

Figs. 5(b) and 5(c). Fig. 5(b) shows excellent agreement in T_{max} separately obtained by RCWA (symbols) and Eq. (9) (curves). Note that M and η_{rad} for T_{max} in Eq. (9) are purely obtained from the absorption spectra.

VI. Decomposition of Total Field into Resonant and Non-Resonant Configurations

The EM field is readily decomposed into configurations associated with two interfering pathways in this theory. For port 1 (air-side) incidence, the total magnetic field can be written as $\mathbf{H}_{tot} = \mathbf{h}_1 - \rho_1 \mathbf{h}_1^* - \tau\ \mathbf{h}_2^* + \mathbf{H}_{QBM}$, where $\mathbf{H}_{QBM}$ is the field associated with the QBM and $\mathbf{h}_n$ is the normalized field for incoming light at port n; thus, $-\mathbf{h}_n^*$ represents the normalized field for outgoing light at port n. We define two orthogonal projection operators Q and P that respectively project a field configuration onto the resonant and non-resonant subspace of a Hilbert space formed by the normalized field solutions of Maxwell's equations. The coupled-mode pictures in Figs. 1(a) and 1(b) derive the resonant configuration $\mathbf{H}_R = Q\ \mathbf{H}_{tot} = a(\kappa_1^* \mathbf{h}_1 + \kappa_2^* \mathbf{h}_2 - \sigma\kappa_1 \mathbf{h}_1^* - \sigma\kappa_2 \mathbf{h}_2^*) + \mathbf{H}_{QBM}$, and non-resonant configuration $\mathbf{H}_D = P\mathbf{H}_{tot} = \mathbf{H}_{tot} - \mathbf{H}_R$, where $a = \kappa_1/(2\gamma_{rad})$ and $\sigma = (\eta_{rad} - \eta_{nr} + i\delta)/(1 - i\delta)$ (see APPENDIX C). Note that $\mathbf{H}_R$ completely describes $\mathbf{H}_{QBM}$ in $\mathbf{H}_{tot}$ and can be obtained by two coherent wave incidences with amplitudes $a\kappa_1^*$ from port 1 and $a\kappa_2^*$ from port 2. On the other hand, if we have incident waves associated with $\mathbf{H}_D$, the QBM is not excited. Fig. 8 presents the RCWA simulation results for these two situations and confirms the validity of the field decomposition based on our theory.

VII. Conclusion

In summary, we developed a quasi-reversible Fano interference theory of the resonance properties of metallic nanoslit arrays that is consistent with the original Fano resonance theory on quantum interference of auto-ionizing atoms. Our formulation captures the essential characteristics of dissipative resonant systems such as the metallic nanoslit arrays treated in this paper. We show that the quasi-reversibility requirement derives the analytic description of the resonant transmission and associated nonreciprocal absorption in terms of a minimal number of independent basic parameters, i.e., partial decay probabilities (η_1 and η_2) and non-resonant transmission amplitude (t_D). With clear definitions of two interfering electromagnetic field configurations and the associated absorbing processes, the theory reveals the essential physics of resonant interference in the EOT phenomenon: (i) the enhanced transmission peak is given by the product of partial decay probabilities ($4\eta_1\eta_2$), independent of the non-resonant expectation $|t_D|^2$; (ii) in a highly asymmetric coupling regime where $4\eta_1\eta_2 \approx |t_D|^2 << 1$, excitation of the QBM leads to an anti-resonant extinction of the transmission indicating a negative role of the QBM; (iii) parity of the QBM determines occurrence of red or blue tails in the spectral profile; (iv) absorbance measurements yield direct determination of the partial decay probabilities by which main features of the resonant transmission are quantitatively explained. Thus, these basic parameters can be directly established experimentally.

Further extension of our theory to a multiple-QBM system may offer concomitant analytic descriptions pertinent to other resonant nanophotonic systems. In guided-mode resonance devices or nanoplasmonic templates, the coupling between localized modes provides a variety of useful spectra including filters [24] and polarizers [25] or a plasmon-induced transparency [26]. We believe that the quasi-reversible interference picture can be applied to such systems as well as others that exhibit general aspects of QBM resonances to further elucidate their essential physics.

APPENDIX

A. Transmission and Reflection Coefficients

Using coupled-mode theory [5], we model an extraordinary optical transmission (EOT) system as a two-port resonant scattering problem assuming the non-resonant pathway to be lossless and include absorption to cause non-radiative decay of the QBM. This is schematically depicted in Fig. 1(b), where $\psi_{n\pm}(t)$ represents amplitudes of the coupled radiation modes at port n (+: incoming mode, −: outgoing mode). For a QBM with amplitude $\Phi(t)$, the modal amplitudes are assumed to describe slowly varying envelopes of corresponding mode fields detailed as follows. The electric ($\mathbf{E}$) and magnetic ($\mathbf{H}$) fields associated with the QBM can be expressed as

$$\mathbf{E}_{\mathrm{QBM}}(\mathbf{r},t)=\Phi(t)\mathbf{e}_{\mathrm{QBM}}(\mathbf{r})e^{-i\omega t}+(C.C) \tag{A1}$$

and

$$\mathbf{H}_{\mathrm{QBM}}(\mathbf{r},t)=\Phi(t)\mathbf{h}_{\mathrm{QBM}}(\mathbf{r})e^{-i\omega t}+(C.C). \tag{A2}$$

The fields associated with the coupled radiation mode are then

$$\mathbf{E}_n(\mathbf{r},t)=[\psi_{n+}(t)\mathbf{e}_n(\mathbf{r})+\psi_{n-}(t)\mathbf{e}_n^*(\mathbf{r})]e^{-i\omega t}+(C.C) \tag{A3}$$

and

$$\mathbf{H}_n(\mathbf{r},t)=[\psi_{n+}(t)\mathbf{h}_n(\mathbf{r})-\psi_{n-}(t)\mathbf{h}_n^*(\mathbf{r})]e^{-i\omega t}+(C.C). \tag{A4}$$

In these equations, $\mathbf{e}_{\mathrm{QBM}}(\mathbf{r})$ and $\mathbf{h}_{\mathrm{QBM}}(\mathbf{r})$ are frequency-domain solutions of Maxwell equations for the QBM while $\mathbf{e}_n(\mathbf{r})$ and $\mathbf{h}_n(\mathbf{r})$ denote the incoming radiation mode at port n. Correspondingly, $\mathbf{e}_n^*(\mathbf{r})$ and $-\mathbf{h}_n^*(\mathbf{r})$ represent the outgoing radiation mode at port n. "$(C.C)$" refers to the complex conjugate. The modal fields are assumed to be normalized such that

$$2\int_V d^3r\left(\frac{1}{2}\frac{d\left(\omega\varepsilon'\right)}{d\omega}|\mathbf{e}_{\mathrm{QBM}}|^2+\frac{1}{2}\mu_0|\mathbf{h}_{\mathrm{QBM}}|^2\right)=1, \tag{A5}$$

$$2\int_{\partial V} d^2\mathbf{r}\cdot Re\left(\mathbf{e}_n\times\mathbf{h}_n^*\right)=1, \tag{A6}$$

where V and ∂V represent a volume containing the QBM and boundary surface of V, respectively. On this basis, we can take $|\Phi|^2$ and $|\psi_{n+}|^2-|\psi_{n-}|^2$ as time-averaged energy content in the QBM and power incoming to the resonator through port n. Defining a non-radiative decay rate by [27]

$$\gamma_{\mathrm{nr}}=\omega\int_V d^3r\,\varepsilon''|\mathbf{e}_{\mathrm{QBM}}|^2, \tag{A7}$$

provides the power absorbed by the QBM as

$$\int_V d^3r\,\omega\varepsilon''\left\langle\left|\mathbf{E}_{\mathrm{QBM}}\right|^2\right\rangle_t=2\gamma_{\mathrm{nr}}U_{\mathrm{QBM}}(t), \tag{A8}$$

where $\varepsilon=\varepsilon'+i\varepsilon''$ is the dielectric constant of material inside V and $\langle\cdots\rangle_t$ denotes the time average of its inner part.

For a QBM resonant at frequency ω_0 in a slowly decaying regime such that $\gamma_{\mathrm{rad}}+\gamma_{\mathrm{nr}}<<\omega_0$, $\Phi(t)$, $\psi_{n\pm}(t)$, and γ_{nr} in Eqs. (A1)–(A4), (A7) satisfy coupled-mode equations [5], [14], [16] given as

$$\frac{d}{dt}\Phi(t)=\left[i(\omega-\omega_0)-\gamma_{\mathrm{rad}}-\gamma_{\mathrm{nr}})\right]\Phi(t)+\left(\langle\kappa|^*\right)|\psi_+(t)\rangle, \tag{A9}$$

$$|\psi_-(t)\rangle=\mathbf{C}\,|\psi_+(t)\rangle+\Phi(t)\,|\kappa\rangle, \tag{A10}$$

where the radiation decay rate is $\gamma_{\mathrm{rad}}=(|\kappa_1|^2+|\kappa_2|^2)/2$ and the non-resonant scattering matrix is

$$\mathbf{C}=\begin{bmatrix} r_1 & t_{\mathrm{D}} \\ t_{\mathrm{D}} & r_2 \end{bmatrix}. \tag{A11}$$

Bra-ket notation represents a column vector $|u\rangle=(u_1u_2)^T$ with its complex-conjugate transpose $\langle u|=(u_1^*u_2^*)$. For stationary excitation in which $d\Phi/dt=0$, the coupled-mode Eqs. (A9) and (A10) are reduced to

$$\Phi=\frac{1}{\gamma_{tot}}\frac{\left(\langle\kappa|^*\right)|\psi_+\rangle}{1-i\delta}, \tag{A12}$$

$$|\psi_-\rangle=\left[\mathbf{C}+\frac{1}{\gamma_{tot}}\frac{|\kappa\rangle\langle\kappa|^*}{1-i\delta}\right]|\psi_+\rangle, \tag{A13}$$

where total decay rate $\gamma_{\mathrm{tot}}=\gamma_{\mathrm{rad}}+\gamma_{\mathrm{nr}}$ and reduced frequency $\delta=(\omega-\omega_0)/\gamma_{\mathrm{tot}}$. By applying $|\psi_+\rangle=(1\ 0)^T$ for port 1 incidence or $|\psi_+\rangle=(0\ 1)^T$ for port 2 incidence to Eq. (A13), we obtain the transmission and reflection coefficients

$$\tau(\delta)=\psi_{\nu-}=t_{\mathrm{D}}+\frac{2\sqrt{\eta_1\eta_2}}{1-i\delta}e^{i\phi}, \tag{A14}$$

$$\rho_n(\delta)=\psi_{n-}=r_n+\frac{2\eta_n}{1-i\delta}e^{i\varphi_n}, \tag{A15}$$

respectively, where n denotes the incident port, ν indicates the transmission port, e.g., $\nu=2$ for $n=1$, partial decay probability $\eta_n=|\kappa_n|^2/2\gamma_{\mathrm{tot}}$, resonant transmission phase $\phi=\arg(\kappa_1)+\arg(\kappa_2)$, and resonant reflection phase at port n $\varphi_n=2\arg(\kappa_n)$.

B. Quasi Reversibility, Amplitude-Phase Correlation, and Nonreciprocal absorption

The source-free frequency-domain Maxwell equations

$$\nabla\cdot\mathbf{E}=0,\ \nabla\cdot\mathbf{H}=0,\ \nabla\times\mathbf{E}=i\omega\mu\mathbf{H},\ \text{and}\ \nabla\times\mathbf{H}=-i\omega\varepsilon\mathbf{E}$$

are invariant under a set of operations that $\mathbf{E}\rightarrow\mathbf{E}^*$, $\mathbf{H}\rightarrow-\mathbf{H}^*$, $\varepsilon\rightarrow\varepsilon^*$, and $\mu\rightarrow\mu^*$ [14], [28]. Note that the set of operations in this case corresponds to not only the time reversal of the field-scattering processes but also to the loss-gain interchange (sign changes in the imaginary parts of ε and μ). Thus, phase-front propagation as well as power flow change direction, i.e., $\mathrm{Re}[\mathbf{E}\times\mathbf{H}^*)\rightarrow\mathrm{Re}[\mathbf{E}^*\times(-\mathbf{H})]=-\mathrm{Re}(\mathbf{E}\times\mathbf{H}^*)$. Therefore, for time-harmonic fields, if a certain incoming field configuration is scattered to the corresponding outgoing field configuration by an object with ε and μ, the time reversal of the outgoing field configuration should be scattered to the time reversal of the originally incoming field configuration by the object with its loss interchanged with gain in the same amount ($\varepsilon\rightarrow\varepsilon^*$ and $\mu\rightarrow\mu^*$). Scattering process by an absorbing object is time reversible under the allowance of loss-gain interchange. However, the loss-gain

interchange at the macroscopic level is physically forbidden by the second law of thermodynamics because it is inevitable that the absorbed energy is thermally redistributed into other quanta in an irreversible way. That is why we use the term "quasi-reversibility" instead of "reversibility" when considering time reversal of the scattering process by an absorbing object such as a metallic structure.

For a general case where N pairs of incoming and outgoing waves are coupled by a scattering process, quasi reversibility can be discussed concisely by using the scattering matrix (S-matrix) formalism. Let $\mathbf{S}$ denote the S-matrix, which relates the incoming and outgoing modes, $|\psi_+\rangle$ and $|\psi_-\rangle$, respectively, by the equation $|\psi_-\rangle = \mathbf{S}|\psi_+\rangle$. Quasi-reversibility requires that time-reversed outgoing waves scatter to the time-reversed incoming waves. The time-reversed situation is obtained by taking $|\psi_+\rangle \rightarrow |\psi_-\rangle^*$ for the incoming wave configuration, $|\psi_-\rangle \rightarrow |\psi_+\rangle^*$ for the outgoing wave configuration, and $\mathbf{S}(\varepsilon) \rightarrow \mathbf{S}(\varepsilon^*)$. This results in the S-matrix equation $|\psi_+\rangle^* = \mathbf{S}(\varepsilon^*)|\psi_-\rangle^*$. By requiring this equation to be identical to the S-matrix equation for the original situation $|\psi_-\rangle = \mathbf{S}(\varepsilon)|\psi_+\rangle$, we obtain

$$\mathbf{S}^*(\varepsilon^*) = \mathbf{S}^{-1}(\varepsilon) \text{ for } \textit{quasi reversibility}. \tag{A16}$$

Note that reciprocity requires the S-matrix to be symmetric; thus, the quasi-reversibility condition of Eq. (A16) is independent of the reciprocity. Also, we note that Eq. (A16) reduces to the well-known condition of reversibility in lossless cases, i.e., $\mathbf{S}^* = \mathbf{S}^{-1}$, as $\mathrm{Im}(\varepsilon)$ approaches zero [5]. Consequently, Eq. (A16) can be considered an extension of reversibility in lossless systems to absorbing systems.

Using Eq. (A13), we find

$$\mathbf{S}(\varepsilon) = \mathbf{C} + \frac{|\kappa\rangle\langle\kappa|^*}{\gamma_{\mathrm{rad}} + \gamma_{\mathrm{nr}} - i(\omega - \omega_0)}, \tag{A17}$$

and

$$\mathbf{S}(\varepsilon^*) = \mathbf{C} + \frac{|\kappa\rangle\langle\kappa|^*}{\gamma_{\mathrm{rad}} - \gamma_{\mathrm{nr}} - i(\omega - \omega_0)}. \tag{A18}$$

Note in Eq. (A18) that $\gamma_{\mathrm{nr}} \rightarrow -\gamma_{\mathrm{nr}}$ according to Eq. (A7) where $\gamma_{\mathrm{nr}} \propto \mathrm{Im}(\varepsilon)$. Here, we assume the non-resonant scattering to be lossless, i.e., $\mathbf{C}^{-1} = \mathbf{C}^\dagger$, and this assumption restricts $\mathbf{C}$ in Eq. (A11) to take the form [5]

$$\mathbf{C} = \begin{bmatrix} -re^{i2\xi_1} & \pm ite^{i(\xi_1+\xi_2)} \\ \pm ite^{i(\xi_1+\xi_2)} & -re^{i2\xi_2} \end{bmatrix}. \tag{A19}$$

For a homogeneous metallic film with a thickness much larger than the skin depth, the Fresnel reflection and transmission formula yields $\xi_n \approx \tan^{-1}[(\varepsilon_n/|\varepsilon_{\mathrm{metal}}|)^{1/2}] << 1$ where $n = 1$ or 2 denotes the ports and take (+) sign for the off-diagonal elements (non-resonant transmission coefficient) under the definition of $\psi_{n\pm}$ based on the EM field configurations in Eqs. (A3) and (A4). Accordingly, it is reasonable to use Eq. (A19) with $\xi_n << 1$ and (+) sign for the off-diagonal elements when describing the non-resonant response of a perforated film possessing sub-wavelength holes or slits.

Applying Eqs. (A17)–(A19) to the quasi-reversibility requirement of Eq. (A16) yields

$$1 + t\sqrt{\eta_\nu/\eta_n}e^{i\Delta} = re^{i\Delta_n}, \tag{A20}$$

where $\Delta = \xi_1+\xi_2+\pi/2-\arg(\kappa_1)-\arg(\kappa_2)$, $\Delta_n = 2[\xi_n-\arg(\kappa_n)]$, and ν is exclusive index as used in Eq. (A14). In connection with $\tau(\delta)$ and $\rho_n(\delta)$ in Eq. (A14) and (A15), respectively, $t = |t_{\mathrm{D}}|$ is non-resonant transmission magnitude, $r_{\mathrm{D}} = |r_n|$ is non-resonant reflection magnitude, $\Delta = \arg(t_{\mathrm{D}})-\phi$ denotes phase difference between the non-resonant and resonant transmission at $\delta = 0$, and $\Delta_n = \arg(r_n)-\varphi_n$ is phase difference between the non-resonant and resonant reflection at $\delta = 0$. By solving Eq. (A20) for $n = 1$ and 2, we finally obtain intensity-phase correlation in the transmission and reflection as

$$\cos\Delta = -\frac{\eta_{\mathrm{rad}}t}{2\sqrt{\eta_1\eta_2}} \text{ and } \sin\Delta = p\sqrt{1-\cos^2\Delta}, \tag{A21}$$

$$\cos\Delta_n = \frac{1}{r}\left(1 + t\sqrt{\frac{\eta_\nu}{\eta_n}}\cos\Delta\right) \text{and} \sin\Delta_n = \frac{t}{r}\sqrt{\frac{\eta_\nu}{\eta_n}}\sin\Delta, \tag{A22}$$

respectively, where the parity factor $p = +1$ for $|\arg(\kappa_1)-\arg(\kappa_2)| < \pi/2$ or -1 for $|\arg(\kappa_1)-\arg(\kappa_2)| > \pi/2$.

The nonreciprocal absorbance is directly obtained by using Eq. (A12) in the absorbing power expression $A_n = 2\gamma_{\mathrm{nr}}|\Phi|^2$ for unit-amplitude light incidence at port n as

$$A_n(\delta) = \frac{4\eta_{\mathrm{nr}}\eta_n}{1+\delta^2}, \tag{A23}$$

where the QBM absorbing probability is $\eta_{\mathrm{nr}} = 1-\eta_1-\eta_2$. The absorbance can be derived by energy conservation that $A_n + |\tau|^2 + |\rho_n|^2 = 1$. By introducing the intensity-phase correlations of Eqs. (A21) and (A22) to Eqs. (A14) and (A15), we arrive at Eq. (A23), showing that the intensity-phase correlations satisfy the energy conservation requirement.

C. Field Decomposition into the Resonant and Non-Resonant Configurations

Here, we describe how the total EM field $\{\mathbf{E}_{\mathrm{tot}}, \mathbf{H}_{\mathrm{tot}}\}$ can be decomposed into the resonant and non-resonant configurations. We define two orthogonal complementary operators Q and P that respectively project a field solution onto the resonant and non-resonant subspaces in a Hilbert space formed by all normalized field solutions of Maxwell's equations for a given system. The resonant configuration given by $\{\mathbf{E}_{\mathrm{R}}, \mathbf{H}_{\mathrm{R}}\} = \{Q\mathbf{E}_{\mathrm{tot}}, Q\mathbf{H}_{\mathrm{tot}}\}$ fully describes excitation of the field associated with the QBM in $\{\mathbf{E}_{\mathrm{tot}}, \mathbf{H}_{\mathrm{tot}}\}$ while the non-resonant configuration given by $\{\mathbf{E}_{\mathrm{D}}, \mathbf{H}_{\mathrm{D}}\} = \{P\mathbf{E}_{\mathrm{tot}}, P\mathbf{H}_{\mathrm{tot}}\}$ does not couple to the QBM at all. According to the definition of modal amplitudes in Eqs. (A1)–(A4), the total field is given by a superposition of fields associated with the port's radiation modes and the QBM as

$$\mathbf{E}_{\mathrm{tot}} = [\underbrace{\psi_{1+}\mathbf{e}_1 + \psi_{2+}\mathbf{e}_2}_{\text{incoming}} + \underbrace{\psi_{1-}\mathbf{e}_1^* + \psi_{2-}\mathbf{e}_2^*}_{\text{outgoing}} + \underbrace{\Phi\mathbf{e}_{\mathrm{QBM}}}_{\text{QBM}}]e^{-i\omega t} + (C.C) \tag{A24}$$

$$\mathbf{H}_{\mathrm{tot}} = [\underbrace{\psi_{1+}\mathbf{h}_1 + \psi_{2+}\mathbf{h}_2}_{\text{incoming}} - \underbrace{\psi_{1-}\mathbf{h}_1^* - \psi_{2-}\mathbf{h}_2^*}_{\text{outgoing}} + \underbrace{\Phi\mathbf{h}_{\mathrm{QBM}}}_{\text{QBM}}]e^{-i\omega t} + (C.C) \tag{A25}$$

In the coupled-mode Eq. (A9) and its stationary form of Eq. (A12), the part of incoming modes that excites the QBM

Φ is obviously the projection of $|\psi_+\rangle$ onto $|\kappa\rangle^*$. Thus, a normalized matrix $|\kappa\rangle^*\langle\kappa|^*/\langle\kappa|\kappa\rangle = (2\gamma_{\mathrm{rad}})^{-1}(|\kappa\rangle\langle\kappa|^*)$ projects the incoming mode onto the resonant configuration, i.e.,

$$Q\,|\psi_+\rangle = \frac{1}{2\gamma_{\mathrm{rad}}}\,(|\kappa\rangle\,\langle\kappa|)^*\,|\psi_+\rangle = a\,|\kappa\rangle^*\,, \tag{A26}$$

where $a = (\kappa_1\psi_{1+}+\kappa_2\psi_{2+})/(2\gamma_{\mathrm{rad}})$. $Q|\psi_+\rangle$ fully describes Φ as $(\langle\kappa|)^*|\psi_+\rangle = (\langle\kappa|)^*Q|\psi_+\rangle$. Accordingly, projection of the outgoing radiation mode onto the resonant configuration is given by the scattered outgoing mode from $Q|\psi_+\rangle$, i.e.,

$$Q\,|\psi_-\rangle = \mathbf{S}Q\,|\psi_+\rangle = a\sigma(\delta)\,|\kappa\rangle\,, \tag{A27}$$

where $\sigma(\delta) = (\eta_{\mathrm{rad}}-\eta_{\mathrm{nr}}+i\delta)/(1-i\delta)$ and $\mathbf{S}$ is the scattering matrix defined in Eq. (A17). On this basis, we finally have the resonant configuration as follows,

$$\mathbf{E}_R = [a(\underbrace{\kappa_1^*\mathbf{e}_1+\kappa_2^*\mathbf{e}_2}_{\text{incoming}}+\underbrace{\kappa_1\sigma\mathbf{e}_1^*+\kappa_2\sigma\mathbf{e}_2^*}_{\text{outgoing}})+\underbrace{\Phi\mathbf{e}_{\mathrm{QBM}}}_{\text{QBM}}]e^{-i\omega t} + (C.C)\,, \tag{A28}$$

$$\mathbf{H}_R = [a(\underbrace{\kappa_1^*\mathbf{h}_1+\kappa_2^*\mathbf{h}_2}_{\text{incoming}}-\underbrace{\kappa_1\sigma\mathbf{h}_1^*-\kappa_2\sigma\mathbf{h}_2^*}_{\text{outgoing}})+\underbrace{\Phi\mathbf{h}_{\mathrm{QBM}}}_{\text{QBM}}]e^{-i\omega t} + (C.C)\,. \tag{A29}$$

The projection onto the non-resonant configuration $P = 1-Q$ is a complementary projector of Q. Thereby, the non-resonant configuration is obtained simply by the relation $\{\mathbf{E}_{\mathrm{D}}, \mathbf{H}_{\mathrm{D}}\} = \{P\mathbf{E}_{\mathrm{tot}}, P\mathbf{H}_{\mathrm{tot}}\} = \{\mathbf{E}_{\mathrm{tot}}, \mathbf{H}_{\mathrm{tot}}\}-\{\mathbf{E}_{\mathrm{R}}, \mathbf{H}_{\mathrm{R}}\}$.

REFERENCES

[1] T. W. Ebbesen, H. J. Lezec, H. F. Ghaemi, T. Thio, and P. A. Wolff, "Extraordinary optical transmission through sub-wavelength hole arrays," *Nature*, vol. 391, pp. 667–669, Feb. 1998.

[2] J. A. Porto, F. J. Garcia-Vidal, and J. B. Pendry, "Transmission resonances on metallic gratings with very narrow slits," *Phys. Rev. Lett.*, vol. 83, pp. 2845–2848, Oct. 1999.

[3] F. J. García-Vidal, L. Martin-Moreno, T. W. Ebbesen, and L. Kuipers, "Light passing through subwavelength apertures," *Rev. Mod. Phys.*, vol. 82, pp. 729–787, Mar. 2010.

[4] Y. Ding, J. Yoon, M. H. Javed, S. H. Song, and R. Magnusson, "Mapping surface-plasmon polaritons and cavity modes in extraordinary optical transmission," *IEEE Photon. J.*, vol. 3, no. 3, pp. 365–374, Jun. 2011.

[5] H. A. Haus, *Waves and Fields in Optoelectronics*. Englewood Cliffs, NJ: Prentice-Hall, 1984, chs. 3 and 7.

[6] C. Genet, M. P. van Exter, and J. P. Woerdman, "Fano-type interpretation of red shifts and red tails in hole array transmission spectra," *Opt. Commun.*, vol. 225, pp. 331–336, Jul. 2003.

[7] M. Sarrazin and J. P. Vigneron, "Optical properties of tungsten thin films perforated with a bidimensional array of subwavelength holes," *Phys. Rev. E*, vol. 68, pp. 016603-1–016603-4, Jan. 2003.

[8] W. Fan, S. Zhang, K. J. Malloy, and S. R. J. Brueck, "Enhanced mid-infrared transmission through nanoscale metallic coaxial-aperture arrays," *Opt. Exp.*, vol. 13, pp. 4406–4413, Jun. 2005.

[9] H. Liu and P. Lalanne, "Microscopic theory of the extraordinary optical transmission," *Nature*, vol. 452, pp. 728–731, Apr. 2008.

[10] H. A. Bethe, "Theory of diffraction by small holes," *Phys. Rev.*, vol. 66, nos. 7–8, pp. 163–182, Oct. 1944.

[11] U. Fano, "Effects of configuration interaction on intensities and phase shifts," *Phys. Rev.*, vol. 124, no. 6, pp. 1866–1878, Dec. 1961.

[12] A. E. Mirochnichenko, S. Flach, and Y. S. Kivshar, "Fano resonances in nanoscale structures," *Rev. Mod. Phys.*, vol. 82, pp. 2257–2298, Aug. 2010.

[13] J. Weiner, "The physics of light transmission through subwavelength apertures and aperture arrays," *Rep. Prog. Phys.*, vol. 72, p. 064401, May 2009.

[14] J. Yoon, K. H. Seol, S. H. Song, and R. Magnusson, "Critical coupling in dissipative surface-plasmon resonators with multiple ports," *Opt. Exp.*, vol. 18, pp. 25702–25711, Nov. 2010.

[15] W. Wan, Y. Chong, L. Ge, H. Noh, A. D. Stone, and H. Cao, "Time-reversed lasing and interferometric control of absorption," *Science*, vol. 331, pp. 889–892, Feb. 2011.

[16] S. Fan, W. Suh, and J. D. Joannopoulos, "Temporal coupled-mode theory for the Fano resonance in optical resonators," *J. Opt. Soc. Amer. A*, vol. 20, pp. 569–572, Mar. 2003.

[17] Q. Cao and P. Lalanne, "Negative role of surface plasmons in the transmission of metallic gratings with very narrow slits," *Phys. Rev. Lett.*, vol. 88, no. 5, pp. 057403-1–057403-4, Jan. 2002.

[18] P. B. Catrysse and S. Fan, "Near-complete transmission through sub-wavelength hole arrays in phonon-polaritonic thin films," *Phys. Rev. B*, vol. 75, no. 7, pp. 075422-1–075422-5, Feb. 2007.

[19] F. J. G. de Abajo, R. Gómez-Medina, and J. J. Sáenz, "Full transmission through perfect-conductor subwavelength hole arrays," *Phys. Rev. E*, vol. 72, pp. 016608-1–016608-5, Jul. 2005.

[20] W. L. Barnes, W. A. Murray, J. Dintinger, E. Devaux, and T. W. Ebbesen, "Surface plasmon polaritons and their role in the enhanced transmission of light through periodic arrays of subwavelength holes in a metal film," *Phys. Rev. Lett.*, vol. 92, no. 10, pp. 107401-1–107401-4, Mar. 2004.

[21] M. G. Moharam and T. K. Gaylord, "Rigorous coupled-wave analysis of planar-grating diffraction," *J. Opt. Soc. Amer.*, vol. 71, pp. 811–818, Jul. 1981.

[22] E. Altewischer, M. P. van Exter, and J. P. Woerdman, "Nonreciprocal reflection of a subwavelength hole array," *Opt. Lett.*, vol. 28, pp. 1906–1908, Oct. 2003.

[23] J. Yoon, S. H. Song, and J.-H. Kim, "Extraction efficiency of highly confined surface plasmon-polaritons to far-field radiation: An upper limit," *Opt. Exp.*, vol. 16, pp. 1269–1279, Jan. 2008.

[24] Y. Ding and R. Magnusson, "Resonant leaky-mode spectral-band engineering and device applications," *Opt. Exp.*, vol. 12, pp. 5661–5674, Nov. 2004.

[25] K. J. Lee, J. Curzan, M. Shokooh-Saremi, and R. Magnusson, "Resonant wideband polarizer with single silicon layer," *Appl. Phys. Lett.*, vol. 98, no. 21, pp. 211112-1–211112-3, May 2011.

[26] N. Liu, L. Langguth, T. Weiss, J. Kästel, M. Fleischhauer, T. Pfau, and H. Giessen, "Plasmonic analogue of electromagnetically induced transparency at the Drude damping limit," *Nature Mater.*, vol. 8, pp. 758–752, Jul. 2009.

[27] L. D. Landau, E. M. Lifshitz, and L. P. Pitaevskii, *Electrodynamics of Continuous Media*, 2nd ed. New York: Elsevier, 1984, pp. 272–276.

[28] A. Lakhtakia, "Conjugation symmetry in linear electromagnetism in extension of materials with negative real permittivity and permeability scalars," *Microw. Opt. Technol. Lett.*, vol. 40, no. 2, pp. 160–161, Jan. 2004.

Jae Woong Yoon received the Ph.D. degree in physics from Hanyang University, Seoul, Korea, in 2006.

He was a Post-Doctoral Fellow with the Department of Physics, Hanyang University from 2006 to 2011. In 2010, he joined the Department of Electrical Engineering, University of Texas-Arlington, Arlington, where he is currently an Assistant Research Professor. His current research interests include passive and active nanophotonic devices and biochemical sensors based on surface plasmon and guided-mode resonances in periodic films.

Myoung Jin Jung received the B.S. degree in physics from Dong-guk University, Seoul, Korea, in 2006, and the M.S. degree in physics from Hanyang University, Seoul, in 2008. He is currently pursuing the Ph.D. degree with the Department of Physics, Hanyang University.

His current research interests include surface-plasmonic waveguides and active plasmonic elements.

Seok Ho Song received the B.S. degree in physics from Yonsei University, Seoul, Korea, in 1984, and the M.S. and Ph.D. degrees in physics from the Korean Advanced Institute of Science and Technology, Seoul, in 1986 and 1989, respectively.

He was a Senior Researcher with Electronics and Telecommunications Research Institute, Daejon, Korea, from 1989 to 1997. In 1997, he became a Professor with the Department of Physics, Hanyang University, Seoul. His current research interests include surface plasmon photonics and grating resonances.

Dr. Song is a member of the Optical Society of America.

Robert Magnusson (M'69–SM'90) received the Ph.D. degree in electrical engineering from the Georgia Institute of Technology, Atlanta, in 1976.

He spent several years in industry and then joined the Faculty of the University of Texas (UT)–Arlington and became a Full Professor in 1992. He served as a Professor and Chair of the Department of Electrical Engineering from 1998 to 2001. He was a Professor and the Head of the Electrical and Computer Engineering Department, University of Connecticut, Storrs Mansfield, from 2001 to 2006, and a Professor from 2006 to 2008. In 2008, he returned to UT–Arlington to serve as the Texas Instruments Distinguished University Chair in Nanoelectronics and a Professor of Electrical Engineering, where he is currently the Director of the Nanophotonics Device Group. He is the Co-Founder and the Chief Technical Officer of Resonant Sensors Inc., Arlington, which is a company that provides next-generation optical sensor systems for medical diagnostics, drug development, and other applications. He has published more than 300 journal and conference papers and holds 16 patents. His current theoretical and experimental research interests include periodic nanostructures, nanolithography, nanophotonics, nanoelectronics, nanoplasmonics, and optical bio- and chemical sensors.

Prof. Magnusson is a fellow of the Optical Society of America and International Society for Optical Engineering (SPIE). He is an Editorial Board Member for the *Journal of ISRN Optics* and the *Journal of Biosensors & Bioelectronics* as well as a Guest Editor for *Nanophotonic Devices*, a special issue in *Micromachines*. He has served as a Topical Editor of *Applied Optics* and as an Associate Editor of *Optical Engineering*. He is the recipient of the IEEE Third Millennium Medal and an Elected Member of the Connecticut Academy of Science and Engineering.